

Green synthesis of Pluronic stabilized reduced graphene oxide: Chemical and biological characterization

Cherian R.S¹, Sandeman S², Ray S³, Savina I.N², Ashtami J¹, Mohanan P.V^{1*}

¹Toxicology Division, Biomedical Technology Wing

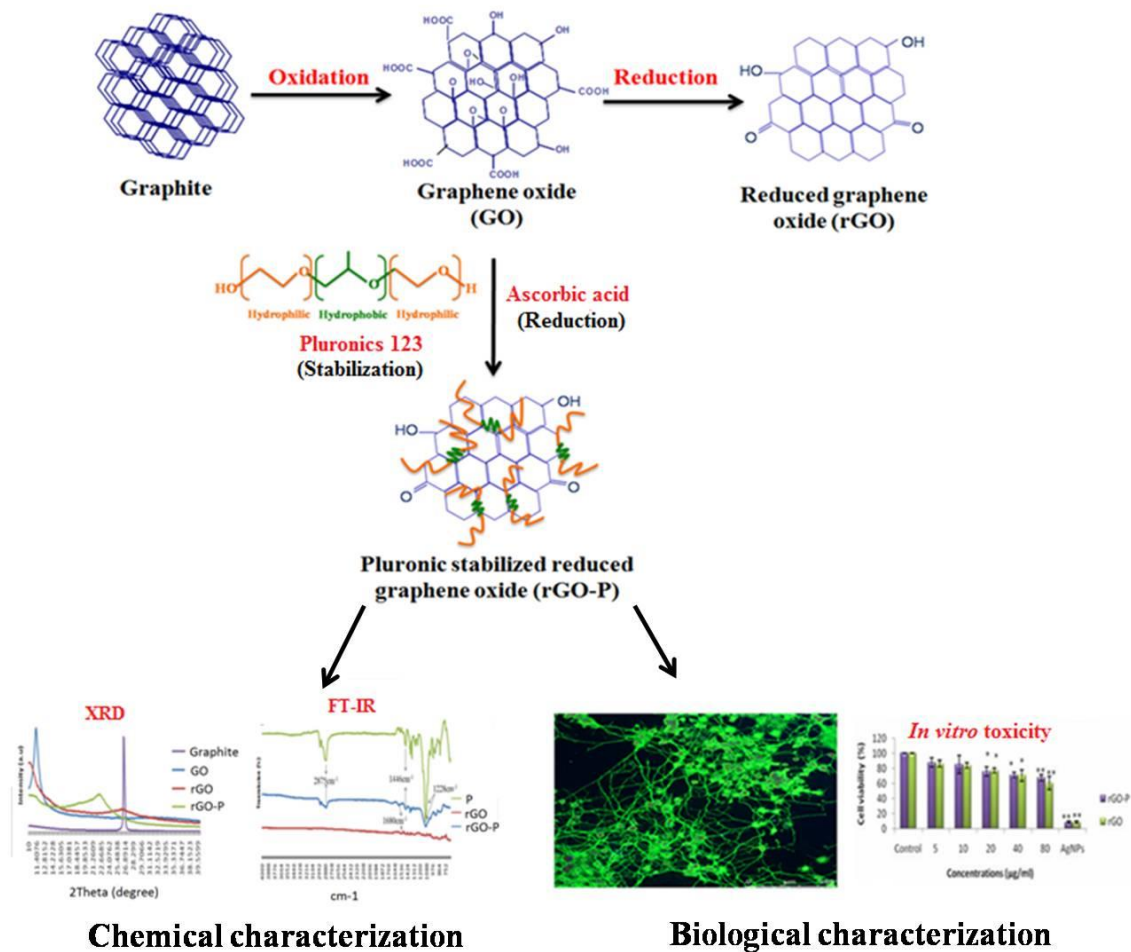
Sree Chitra Tirunal Institute for Medical Sciences and Technology,
Thiruvananthapuram 695 012, Kerala, India

²Biomaterials Research Group, School of Pharmacy and Biomolecular Sciences,
University of Brighton, Brighton, East Sussex, BN2 4GJ, UK

³Surface Analysis Laboratory, School of Environment and Technology,
University of Brighton, Brighton, East Sussex, BN2 4GJ, UK

* Corresponding Author: PV. Mohanan: mohanpv10@gmail.com

Graphical abstract



Highlights

- Green Synthesis of reduced graphene oxide
- Pluronic stabilization
- Physico-chemical characterization
- Biological characterization

Abstract

The wonder material graphene has numerous potential applications in nanoelectronics, biomedicine, storage devices, *etc.* Synthesis of graphene is highly challenging due to the toxic chemicals used and its low yield. In the present study, a facile green route of synthesis of reduced graphene oxide (rGO) was carried out using ascorbic acid as reducing agent. rGO was stabilized using Pluronic P123 polymer to give Pluronic stabilized reduced graphene oxide (rGO-P) and gave superior yield (15mg graphene oxide yielded ~13mg rGO-P). Despite the

potential neuroscience applications of graphene, the impending toxicological outcome upon interaction with neurons is not well understood. Here, differentiated PC-12 neuron-like cells exposed to rGO-P showed a dose-dependent cytotoxicity. Membrane disruption and cytoskeletal integrity remained uncompromised after 24h exposure. Oxidative stress in PC-12 was evident due to an increase in ROS generation in dose and time-dependent manner. *In vivo* acute toxicity was assessed in mice administered with 10mg/kg body weight of rGO-P. There were no evident changes in behaviour, motor function or other morphological changes. In conclusion, rGO-P was successfully synthesized and provided superior yield. Even though *in vitro* toxicity testing showed dose-dependent toxicity, *in vivo* toxic effect was not apparent.

Keywords: graphene; neurotoxicity; Nanoparticles; toxicity; BBB; Pluronic

1. Introduction

Over the past decade, the steady rise in prominence of graphene in the field of nanomaterial science is attributed to its unique properties. Graphene is an allotrope of carbon-containing sp^2 hybridized carbon atoms that are arranged in a honeycombed lattice network [1]. Graphene has excellent electrical and thermal properties, exceptional mechanical strength and superior optical transmittance [2]. These characteristic properties of graphene have potential application in electronics, storage devices, sensors and biomedicine [3]. The 2D structure of graphene is advantageous especially in drug delivery applications since it facilitate multiple pay load. Electrostatic interaction and π - π conjugation ability of graphene make possible conjugation of aromatic molecules, various drug molecules, as well as biomolecules. The photothermal efficiency and wide possibilities for functionalizations to facilitate effective targeting makes graphene ideal for both diagnostics and treatment. Graphene can also be conjugated to other nanoparticles including quantum dots forming nanocomposite to achieve enhanced

functionalities for various biomedical applications [4,5]. Literature updates reports that GO as effective nanosystem for cancer theranostics. Functionalized graphene modified electrodes have been reported as effective tool for early detection of carcinoma cells [6].

Graphene can be synthesized by different methods. Among them, mechanical exfoliation of highly ordered pyrolytic graphite, epitaxial growth and chemical vapour deposition (CVD) yields graphene of high to appreciable quality with desired electrical properties [7]. However, these techniques require sophisticated instrumentation and are time consuming and expensive for large scale production. Reduction of graphene oxide (GO) yield chemically derived graphene also known as reduced graphene oxide (rGO). rGO is gaining popularity since it can be synthesized by facile, inexpensive and cost effective way making it an obvious choice for large scale synthesis of graphene. The major aim of reduction is to produce the electrical properties similar to pristine graphene. Different strategies for rGO synthesis include thermal reduction, chemical reduction using reducing agents like hydrazine hydrate, sodium borohydride, ascorbic acid, biological reduction using bacteria and plant extracts [8]. Even though hydrazine hydrate is used widely for graphene oxide reduction, it is highly poisonous and explosive and therefore demands precaution while handling. On the other hand, use of ascorbic acid as reducing agent provides mild reaction condition avoiding the use of harmful reducing agents. Ascorbic acid is reported to be the first eco-friendly agent for reducing GO and turns out to give good result compared to toxic hydrazine hydrate. Zhang *et al* reported the effective reduction of graphene oxide using L-ascorbic acid. The obtained reduced graphene oxide showed appreciable electronic conjugation state of reduced graphene oxide similar to that obtained from reduction using hydrazine hydrate. As per the literature, ascorbic acid are reliable and harmless reducing agent for reduction of graphene oxide to reduced graphene oxide [9]. As per earlier studies ascorbic acid reduced graphene oxide is optimal for various

applications. Ascorbic acid facilitates fast reduction of graphene oxide at a controllable, cheaper and efficient way [10].

Upon reduction of GO, rGO becomes hydrophobic due to the removal of oxygen functional groups. This causes rGO to aggregate in aqueous solution and hampers biomedical applications that require a stable dispersion of rGO. Numerous methods are employed for the dispersion of rGO which include using surfactants, non-covalent functionalization with dextran [11], Pluronic [12] and covalent binding of polymers like PEG [13], PVA [14] *etc.* Functionalization also helps to improve the biocompatibility and reduce associated toxicity. Graphene can be functionalized either covalently or non-covalently by using various polymers like polyethylene glycol (PEG), dextran, pluronics *etc.*, and biomolecules [15]. Pluronic is a triblock copolymer, (poly(ethylene oxide)-block-poly(propylene oxide)-block-poly(ethylene oxide)). Pluronic copolymer functionalization yield graphene with good colloidal stability since hydrophobic part of pluronics, poly(propylene oxide) segment bind to hydrophobic part of graphene while the hydrophilic poly(ethylene oxide) extend into water [16].

With the advancement in graphene synthesis and application, more concern about the health risk upon exposure to these nanomaterials is rising [17]. Before commercialization of these nanomaterials, a comprehensive understanding of its interaction with the biological system is warranted. Graphene has numerous prospective neurotherapeutic applications like neuroregeneration, tumor therapy and deep brain stimulation [18]. There is a remarkable hike in investigation on scope of GO for various health care applications notably for drug delivery, cancer theranostics, PDT, neuroregeneration, anti-HIV and anti-bacterial activity. Functionalized GO is reported to cross blood brain barrier (BBB) and successfully induce photothermal effect in a particle concentration and radiant dependent manner. Therefore graphene is reputedly a widely researched material for photothermal treatment of alzheimer's

disease [19]. Even though there are several studies on the neurotoxic potential of graphene [20]., the rGO effects on central nervous system has been so far poorly explored [21]. Therefore studying the interaction of graphene with neurons is essential for risk assessment. In this background, this study holds significance.

The current study employed a novel eco-friendly route of synthesis of rGO. Here a green reductant, ascorbic acid was used for the reduction of GO to rGO. The synthesized rGO was dispersed using a tri block co-polymer, Pluronic P123, to form Pluronic stabilized reduced graphene oxide (rGO-P). Since graphene has applications in the field of neuroscience, PC-12 cells were chosen as the test system. PC-12 cells are a rat pheochromocytoma cell line that is responsive to NGF and differentiates into neuron like cells. Cytotoxicity was assessed in PC-12 cells differentiated into neurons by nerve growth factor (NGF). *In vivo* acute toxicity was also carried out in Swiss Albino mice.

2. Materials and methods

2.1 Material

Graphite (Acros organic, Belgium), Potassium permanganate (Fisher Scientific, USA). Ascorbic acid, Pluronic P123 (Mn-5800), RPMI-1640, horse serum (HS), fetal bovine serum (FBS), type IV collagen, NGF- β , 2',7'-dichlorofluorescein diacetate (DCFH-DA) were purchased from Sigma (USA). CellTiter 96[®] Aqueous One Solution Cell Proliferation Assay [MTS] and CytoTox 96[®] Non-Radioactive Cytotoxicity Assay (LDH) were procured from Promega (USA). Anti-beta III tubulin antibody ab18207, Goat Anti-rabbit IgG H&L (Alexa Fluor 488) ab150077 were obtained from Abcam (UK).

2.3 Methods

2.3.1 Synthesis of reduced graphene oxide (rGO)

rGO was synthesized by the reduction of GO using ascorbic acid. GO was prepared using Hummer's method [22] by exfoliating graphite in potassium permanganate and sulphuric acid. GO solution (1mg/ml) was bath sonicated using (Bandelin sonorex R100H) for 30min. 2mM of ascorbic acid was added to the solution and stirred at 95°C for 2h in a water bath. The brown GO solution is reduced by ascorbic acid to a black rGO aggregate. The black precipitate was washed several times in de-ionized water.

2.3.2 Synthesis of Pluronic stabilized reduced graphene oxide (rGO-P)

15ml of GO solution (1mg/ml) was bath sonicated for 30min. It was mixed with 800mg of Pluronic P123 and bath sonicated further for 30min. Ascorbic acid (2mM) was added to the solution and kept for 2h at 95°C in a water bath. Subsequently, the particles were washed thrice with water and bath sonicated (Bandelin sonorex R100H) for 3h for dispersing [23].

2.3.3 Physico-chemical characterization

Characterization of the materials (graphite and GO, rGO and rGO-P) performed using Fourier Transform Infrared Spectroscopy (FTIR), Raman spectroscopy and X-ray Photoelectron Spectroscopy (XPS), Thermogravimetric analysis (TGA), X-ray Diffraction (XRD) and Transmission Electron Microscopy (TEM).

2.3.4 Fourier Transform Infrared Spectroscopy

FTIR spectroscopy is associated with the vibrational energy of atoms or group of atoms in a material. It was utilized to understand the reduction efficiency of GO to rGO and to confirm the stabilization of rGO with Pluronic P123. Graphite, GO, rGO and rGO-P were dried and made into a fine powder. FTIR spectra were recorded using Spectrum 65 FT-IR spectrometer (Perkin Elmer, USA).

2.3.5 Raman Spectroscopy

Raman spectroscopy was carried out to determine the structural and electrical properties of the nanomaterials (Graphite, GO, rGO and rGO-P). Raman spectra was recorded with WITec alpha300 (Germany) using 532 laser with 1s integration time.

2.3.6 X-ray Photoelectron Spectroscopy

XPS analysis was carried out to study the elemental composition of the nanomaterials. XPS was performed using ESCALAB 250Xi system (Thermo Scientific) equipped with a monochromated Al K α X-ray source, a hemispherical electron energy analyzer, a magnetic lens and a video camera for viewing the analysis position. Uniform charge neutralization was provided by beams of low-energy (≤ 10 eV) Ar⁺ ions and low-energy electrons guided by the magnetic lens. The standard analysis spot of ca. 900 \times 900 μm^2 was defined by the microfocus X-ray source. Wide scans (step size 1 eV, pass energy 200 eV, dwell time 10ms) and narrow scans (step size 0.1 eV, pass energy 20 eV, dwell time 50ms) of the C1s (BE \sim 285 eV) and O1s (BE \sim 531 eV) regions were acquired from three separate areas on each sample. Data were transmission function corrected and analyzed using Thermo Avantage Software (Version 5.952) using a smart background.

2.3.7 Thermogravimetric analysis

TGA analysis was carried out to analyze the efficiency of reduction of GO to rGO and rGO-P. It assesses the weight loss of a material as a function of temperature under controlled atmosphere. Samples (graphite, GO, rGO and rGO-P) were analyzed in a nitrogen atmosphere at a temperature range of 100-800 $^{\circ}\text{C}$ in SDT-2960 simultaneous DTA-TGA equipment (TA instruments, USA)

2.3.8 X-ray Diffraction

XRD was carried out to assess crystalline characteristics of graphite, GO, rGO and rGO-P. This was analyzed by Analytical X'Pert Pro MRD (Netherlands).

2.3.9 Transmission Electron Microscopy

TEM analysis was carried out to assess the morphology of rGO-P. Suspensions of the nanomaterials were drop casted on grids and air dried. Samples of rGO-P were analyzed using JEOL JEM 2100 TEM (China).

2.3.10 Dynamic light scattering (DLS)

DLS was used to assess the hydrodynamic size and poly dispersity index (PDI) of rGO-P. This was carried out using Malvern Zetasizer Nano ZS (UK).

3. Biological characterization

3.1 Endotoxin content

Endotoxin content of the rGO and rGO-P was assessed using Charles River Endosafe PTS kit. Nanomaterials (100µg/ml of rGO and rGO-P) were prepared in endotoxin free water. These particles were centrifuged at 14000 rpm for 15 min. The supernatant was assessed for endotoxin contamination. 25 µl of the supernatant was added to the well of the cartridge and loaded on to the Endosafe PTS. Readings were taken and expressed in EU/ml.

3.2 Protein corona

Protein corona preparation was carried out as per Jedlovszky-Hajdu *et al* [24]. rGO and rGO-P (0.04 and 1mg/ml) was used for protein corona identification. The nanomaterials were mixed with 55% v/v (protein concentration in bloodstream) and 10% v/v (protein concentration in *in vitro* cell experiment) of FBS. The aliquots were incubated at 25°C for 1h. After incubation, the particle-protein corona complex was isolated by centrifuging at 20000g for 30 min at 4°C. The protein concentration in the supernatant was estimated using Lowry method [25]. The pellet was washed thrice in PBS at 4°C by centrifuging at 20000g for 30min. Particle-protein corona was resuspended in SDS gel loading buffer and stored at -20°C until further use. The particle-corona complex in gel loading buffer was heated at 100°C for 5 min. Samples were loaded in 12% SDS-PAGE gels and run at a voltage of 8 V/cm for stacking gel and 15 V/cm

for resolving gel. The gel was stained with Coomassie brilliant blue staining. Images were taken in a Bio Imaging system (Syngene, UK).

3.3 Cell culture

3.3.1 PC-12 cell culture and differentiation

PC-12 cells were procured from the institute, Public Health England. PC-12 cells were cultured as a suspension culture in RPMI-1640 media supplemented with 10% heat inactivated horse serum and 5% heat inactivated fetal bovine serum (FBS). For differentiation, PC-12 cells were plated on to type IV collagen coated (0.01% collagen in 0.1M acetic acid) flasks. The cells were grown in RPMI-1640 containing 1% horse serum and supplemented with 50ng/ml of NGF- β from rat for 7 days.

3.3.2 Nanomaterial preparation for cell culture and dosing

Differentiated PC-12 cells were treated with the extract of rGO and rGO-P for various assays. The nanomaterial was extracted (1mg/ml of rGO and rGO-P) in complete tissue culture media (RPMI-1640 with 10% horse serum and 5% FBS) and incubated at 37°C in a shaking incubator for 8h and 24h. The media was centrifuged at 10000rpm for 15 min to pellet the nanomaterial. The supernatant was used for cell culture. 1mg/ml of silver nanoparticle (AgNP) in media was used as positive control. 1mg/ml of nanomaterial (rGO and rGO-P) in media was taken as the stock solution for the direct contact assay. Different concentrations (5, 10, 20, 40 and 80 μ g/ml) was added directly to the cells and incubated for 4h or 24h depending on the assay. AgNP induces high oxidative stress causing damage to major organelles like lysosomes, nucleus and mitochondria. AgNP (100 μ g/ml) was used as positive control [26].

3.4 Cytotoxicity

3.4.1 MTS assay

5×10^4 PC-12 cells were seeded on to 96 well plates and allowed to differentiate for 7 days. For assessing the toxicity of extracts, the media was removed and the cells were incubated with 8h and 24h extract of the rGO, rGO-P and AgNP for a period of 24h. For direct contact MTS assay, the cells were treated with varying concentrations of rGO and rGO -P (5, 10, 20, 30 and 80 μ g/ml) for 24h. Particle blank reading was subtracted from corresponding treated cell reading so as to eliminate the effect of particle alone. Differentiated PC-12 cells treated with 100 μ g/ml of AgNP for 24h was kept as the positive control. The media was aspirated 24h later and 100 μ l of MTS reagent was added and incubated for 2h. Reading was taken at 490nm using a plate reader (Biotek Elx800, USA).

3.4.2 Lactate Dehydrogenase (LDH) assay

PC-12 cells were seeded on to 96 well plates and allowed to differentiate for 7 days. The 8 and 24h extract of rGO and rGO-P were exposed to PC-12 cells for 24h. The direct contact assay was carried out by treating with varying concentrations of rGO and rGO-P (5, 10, 20, 40 and 80 μ g/ml) for 24h. Lysed cells were taken as the positive control. The cells were lysed by adding 10 μ l of lysis solution approximately 2h before adding LDH substrate. 50 μ l of the supernatant was transferred to a fresh plate after 24h and the LDH substrate (50 μ l/well) were added and incubated for 30-45 min. 50 μ l stop solution was added to each well and the reading was taken using a plate reader at 490nm (Biotek Elx800, USA).

3.5 Cellular morphology

3.5.1 Cytoskeletal integrity

Cytoskeletal integrity of PC-12 cells after treatment with nanomaterials was assessed by β -III-tubulin. Cells were seeded on to chambered slides and allowed to differentiate for 7 days in the presence of NGF. The cells were treated with rGO and rGO-P for 24h. Treated cells were fixed

and stained as per manufacturer's instructions. The cells were observed using a confocal microscope (Leica TCS-SP5 Confocal, Germany).

3.6 Free radical production

3.6.1 Reactive oxygen species (ROS) generation assay

PC-12 cells were seeded and allowed to differentiate for a period of 7 days. Media was removed and the cells were washed with PBS gently followed by treatment with 10 μ M of DCFH-DA for 30 min. The DCFH-DA was aspirated out and the cells were rinsed with PBS thrice. Subsequently, the cells were treated with rGO and rGO-P (5, 10, 20, 40 and 80 μ g/ml) for 4h and 24h. After the incubation period, reading was taken in a fluorescent plate reader with excitation at 485nm and emission at 520nm (Biotek Gen 5, USA). 100 μ M of H₂O₂ was added and as a positive control.

3.7 Acute toxicity studies

3.7.1 Animal husbandry and welfare

Swiss Albino mice were procured from the Division of Laboratory Animal Sciences, Biomedical Technology Wing, Sree Chitra Tirunal Institute for Medical Science Technology (Govt. of India), Trivandrum. Acute toxicity studies were carried out in healthy Swiss Albino mice of body weight 20-25g. The animals were maintained in a 12h light and dark cycle with a constant temperature of 22 \pm 2 $^{\circ}$ C and relative humidity of 30-70%. Animals were provided with standard pellet diet and water *ad libitum*. Individual animals were identified by marking with picric acid. Additionally, each animal cage was identified with labels containing details like experiment number, name, animal number(s), date of experiment and end of experimental period. All the animals were acclimatized for a period of 5 days before the start of the experiment. The health of animals was routinely monitored by visual observation. All the animals were handled humanely, without causing any pain or distress with due care for their welfare. The care and management of the animals were carried out in compliance with the

regulations of Committee for the Purpose of Control and Supervision of Experiments on Animals (CPCSEA). All the experiments were carried out after getting the approval from the Institute Animal Ethics Committee (IAEC)(IAEC approval No: SCT/IAEC-073/AUGUST/2013/81;SCT/IAEC-069/AUGUST/2013/81; SCT/ IAEC-176/JANUARY/2016/89).

3.7.2 In vivo acute toxicity studies

Healthy Swiss Albino mice weighing around 20-30g were taken for the study. Mice of age 3-4 weeks were selected for the study. The animals were randomly divided into groups (n=3) of control and test. Mice were injected through intravenous (i.v.) and intraperitoneal (i.p.) route. Animals were injected 10mg/kg body weight of rGO-P in 1ml saline *via* the tail vein (i.v.) or peritoneal cavity (i.p.). Control animals were injected with 1ml saline. 50ml/Kg body weight is the dose approved by USP (United States Pharmacopeia) and ISO 10993-part 11. So, average 20g mice received 1ml of saline. The dose is selected as per the regulatory guidelines. Mice of weight between 17 to 23g were selected. The animals were observed for a period of 72h. The injected mice were observed for a period of 72h for clinical symptoms like change in skin and fur, eyes and mucous membrane, change in behaviour patterns, piloerection, salivation, problems in respiratory, circulatory and nervous systems. The body weight change of the animal was also monitored shortly before the rGO-P was administered *via* i.v./i.p. and at the end of the study (72h).

3.8 Statistical analysis

All the measurements were collected in triplicate and expressed as mean \pm standard deviation (SD). For statistical analysis, the comparison between experimental group and control was carried out using Student's *t*-test. $p \leq 0.05$ was considered significant for all the analysis.

4. Results

4.1 Synthesis of rGO and rGO-P

rGO was synthesized from GO using an environmentally friendly reducing agent - ascorbic acid. Figure 1a shows the process by which reduction removed oxygen groups from GO and resulted in the formation of black rGO aggregates. In order to form stable colloidal suspension Pluronic P123 was incorporated during the reduction process to form rGO-P. Inset of Figure 1a shows that rGO-P maintained colloidal stability and resulted in a uniform black solution in comparison to aggregated rGO.

4.2 Physico-chemical characterization

The reduction efficiency and presence of Pluronic P123 in rGO-P was analyzed using FTIR. The FTIR spectra of graphite, GO and rGO is represented in Figure 1e. Graphite showed no significant peak. The FTIR spectra of GO showed numerous peaks at $\sim 3575\text{cm}^{-1}$ (O-H stretching), $\sim 1720\text{cm}^{-1}$ (C=O stretching), $\sim 1680\text{cm}^{-1}$ (C=C vibration) and $\sim 1046\text{cm}^{-1}$ (C-O stretching). The characteristic GO peaks were weakened after reduction with ascorbic acid to rGO. The peak at $\sim 1680\text{cm}^{-1}$ (C=C vibration) remained whereas the peak at $\sim 1720\text{cm}^{-1}$ (C=O stretching) disappeared upon reduction. Presence of a weak peak at $\sim 1046\text{cm}^{-1}$ (C-O stretching) was noticed in rGO. The rGO was stabilized by incorporating Pluronic P123 during the reduction process. Similar results were observed in a study by Choi *et al* [27] and Xu *et al* [28]. Figure 1d shows characteristic peak $\sim 2875\text{cm}^{-1}$ (C-H stretch), $\sim 1446\text{cm}^{-1}$ (C-H bending vibration) and $\sim 1228\text{cm}^{-1}$ (C-H twist) corresponding to Pluronic P123 in rGO-P. This agrees with the study by Pudukudy and Yaakob [29] and confirms the presence of Pluronic P123 in rGO-P. rGO-P also showed a peak at $\sim 1680\text{cm}^{-1}$ corresponding to the C=C stretching of unmodified graphitic domain suggesting the sp^2 lattice was unaltered.

Raman spectra of all the samples exhibited three characteristic peaks – D band, G band and 2D band (Figure 2a-d). D, G and 2D band of graphite was seen at $\sim 1330\text{cm}^{-1}$, $\sim 1558\text{cm}^{-1}$ and

$\sim 2683\text{ cm}^{-1}$. Prominent G band can be seen for GO, rGO and rGO-P at $\sim 1585\text{ cm}^{-1}$, $\sim 1573\text{ cm}^{-1}$ and 1577 cm^{-1} due to the phonon scattering of graphitic structures. The G band is an in-plane vibrational mode of sp^2 hybridized carbon atoms. The D band represents a ring breathing mode from sp^2 carbon atoms that are adjacent to the edge or defect site in graphitic plane. The 2D band represents the double resonant scattering of zone boundary phonons [30]. It was seen that highly ordered graphite shows a strong peak due to the in-plane vibration of graphite lattice ($\sim 1558\text{ cm}^{-1}$) and a weak disorder band caused due to graphite edges ($\sim 1330\text{ cm}^{-1}$) [31]. GO and rGO showed distinctive D band at $\sim 1354\text{ cm}^{-1}$ and $\sim 1334\text{ cm}^{-1}$ whereas G band was visible at $\sim 1585\text{ cm}^{-1}$ and $\sim 1573\text{ cm}^{-1}$ respectively due to the phonon scattering of graphitic structures. A shift back in the peaks ($\sim 12\text{ cm}^{-1}$ red-shift of G peak with respect to GO) in ascorbic acid reduced rGO and rGO-P suggest the self-healing of the graphitic plane upon reduction [30]. The GO samples showed a prominent D peak ($\sim 1354\text{ cm}^{-1}$) in sharp contrast to the small D peak in graphite indicating significant structural disorder due to oxidation. The peak of 2D band was visible at $\sim 2875\text{ cm}^{-1}$ for GO and $\sim 2679\text{ cm}^{-1}$ for rGO. The 2D band ($\sim 2700\text{ cm}^{-1}$) provides information on the layer number of graphitic materials. In case of rGO-P peaks at $\sim 1322\text{ cm}^{-1}$, $\sim 1577\text{ cm}^{-1}$ and $\sim 2672\text{ cm}^{-1}$ represented the D, G and 2D band respectively.

XPS is a surface sensitive analytical technique and is useful in determining the chemical environment of an atom or molecule. The elements present in graphite, GO, rGO and rGO-P and its chemical state were identified using XPS. The survey scans analysis from 1300 eV to 0 eV of graphite, GO rGO and rGO-P (shown in Figure 3a) were performed. Peaks at $\sim 285.0\text{ eV}$ (C1s) and 530.0 eV (O1s) were visible from the broad scan survey. Table 1a shows the atomic percentage of oxygen and carbon. The peak area calculation of carbon to oxygen ratio (C/O) from the XPS spectra survey scan was 46.12 (graphite), 1.88 (GO), 7.30 (rGO) and 3.78 (rGO-P). As the polymer has a C/O ratio around 2.70, it contributed to the decrease of the C/O ratio from 7.30 (rGO) to 3.78 (rGO-P). This suggests that the rGO-P was efficiently stabilized by

Pluronic P123. XPS narrow scan spectra provide the bonding environment of individual elements. In the case of graphite, C1s core spectrum analysis indicated the presence of a prominent peak at ~284.5eV that is attributed to the presence of sp² hybridized carbon atom. Also, few sp³ hybridized hydrocarbons normally appear in graphite. Figure 3b represents the C1s core spectrum analysis of graphite, GO, rGO and rGO-P. The C1s core spectrum analysis showed a prominent peak at ~284.5eV (sp² hybridized carbon atom) for graphite. GO C1s core spectra showed two intense peaks at ~284.5eV (sp² hybridized carbon atom) and ~285.0eV (sp³ hybridized carbon atom). Additional peak at ~286.5 (hydroxyl or epoxy group C-O), ~288.9eV (carboxyl O=C-OH) and ~287.0eV (carbonyl group C=O) was also visible in GO. The rGO and rGO-P C1s core spectrum analysis is shown in Figure 3b. C1s spectra of rGO showed an intense peak at ~284.5eV (sp² hybridized carbon atom) and weak peaks at ~286.0eV (hydroxyl or epoxy group C-O) and ~288.9eV (carboxyl O=C-OH). A prominent peak at ~284.5eV (sp² hybridized carbon atom) was noticed in rGO-P sample. Similarly, a second intense band around ~285.0eV (sp³ hybridized carbon atom) was seen in the C1s core spectrum of rGO-P. Peak of less intensity was also seen at ~287.0eV (C-C-O) and ~288.9eV (O=C-O) in rGO-P.

Thermal stability and reduction efficiency was monitored using TGA. The TGA curve of graphite, GO, rGO and rGO-P is represented in Figure 2 e-h. Graphite showed a weight loss beyond 600°C. In GO a slight weight loss from room temperature to 150°C and a significant weight loss between 150 - 200°C was observed. This is attributed to the removal of oxygen functional groups present in GO thereby releasing CO, CO₂ and steam [32]. The weight loss of rGO was observed from 400°C onwards. Similarly, a sharp decrease in weight at 400°C was observed for rGO-P. In the case of rGO-P samples, the intensity of sp² is higher than that of sp³ indicating the high quality of resulting graphene sheets. A second intense band around ~286.5 eV is ascribed to the presence of C-O group due to Pluronic P123. rGO-P sample

contains less intense peak of residual oxygen groups at ~287.2 eV (carbonyl group C=O) and ~288.9eV (carboxylic acid O=C-OH).

XRD was utilized to monitor the efficiency of the reduction process. The XRD pattern of graphite, GO, rGO and rGO-P is shown in Figure 1c. The characteristic peak of graphite, GO and rGO was observed at ~26.5°, ~11.3° and ~26.4° respectively. This corresponds to an interlayer spacing of 0.35nm, 0.777nm and 0.336nm. rGO-P showed a distinct peak at ~22.16° which corresponds to an interlayer spacing of 0.401nm.

Surface topographic analysis of rGO-P was assessed using TEM. The wrinkled and scrolled appearance of rGO-P is visualized in Figure 1b. The micellar formation of Pluronic P123 is also seen attached to the rGO-P sheets.

4.3 Biological characterization

Nanomaterials should be assessed for the presence of endotoxin in order to eliminate the erroneous interpretation of results. The endotoxin level was ≤ 0.05 EU/ml for rGO and rGO-P as shown in Table 1b.

The biological fate of nanomaterials within living system is understood by studying the protein corona [33]. Surface of nanomaterials is modified by selective adsorption of biomolecules such as protein and lipid upon entry into the biological system. This leads to protein corona formation and provides a biological identity for the nanomaterial. The hard corona was isolated after the nanomaterials (rGO and rGO-P) were incubated with different concentrations of FBS. rGO and rGO-P in different concentrations, relevant for *in vitro* and *in vivo* applications were taken – 0.04mg/ml and 1mg/ml. rGO and rGO-P were incubated with 55% FBS (protein concentration in the bloodstream) and 10% FBS (protein concentration in *in vitro* cell culture). Following incubation with rGO and rGO-P, the protein concentration in the supernatant was estimated using the BSA standard curve. The Figure 4 a and b shows the amount of protein in

the supernatant decreased as the concentration of the nanomaterials increased. rGO promoted more adsorption of proteins when compared to rGO-P. SDS-PAGE was carried out with the particle-protein corona complex to resolve the proteins. A prominent band between 64 and 98kDa was observed in the rGO samples (Figure 4c). On the contrary, rGO-P samples showed no visible band.

4.4 Cytotoxicity

4.4.1 MTS assay

The toxicity of nanomaterials may be due to direct contact of the nanomaterial with the cell or due to remnants of chemical synthesis that leach out into the biological solution thereby affecting the normal functioning of cells. Mitochondrial activity of live cells was assessed using MTS assay. Differentiated PC-12 cells were incubated with extracts (8h and 24h) of rGO and rGO-P for 24h and their viability is shown in Figure 4d. The viability of PC-12 cells treated with rGO and rGO-P extracts were comparable to that of the control. The extract from AgNP (positive control) showed a marked decrease in cell viability in comparison to the negative control due to the silver ions.

The direct contact MTS assay indicated a dose dependent decrease in PC-12 cell viability after treatment with rGO and rGO-P (Figure 4e). The results were statistically significant (from 20 μ g/ml onwards for rGO and rGO-P) with respect to the negative control. As predicted, the positive control (AgNP) showed a drastic loss in viability when compared to the negative control.

4.4.2 LDH assay

Any damage to the cell membrane results in leakage of LDH into the surroundings. The differentiated PC-12 cells were treated for 24h with the 8h and 24h extract of nanomaterials (rGO and rGO-P). Lysed cells were kept as positive control. LDH release in rGO and rGO-P

was comparable to the untreated samples (Figure 4f). Lysed cells (positive control) showed a statistically significant increase in LDH release when compared to control.

PC-12 cells were also directly incubated with various concentrations of rGO and rGO-P and LDH release is shown in Figure 4g. In comparison to the control a discernible increase in LDH release was noticed in PC-12 cells after 24h incubation with rGO. Statistical significance was observed at concentrations of $\geq 20\mu\text{g/ml}$. However, rGO-P did not show any discernible increase in LDH release compared to the negative control.

4.5 Morphological analysis

4.5.1 Cytoskeletal integrity

The effect on cytoskeleton (β -III-tubulin) of PC-12 upon 24h exposure to rGO and rGO-P were assessed using confocal microscope. A slight disintegration of the neurites were observed in rGO (40 and $80\mu\text{g/ml}$) exposed cells (Figure 5). Exposure to rGO-P for 24h did not cause any change in cytoskeletal integrity in PC-12 cells.

4.6 ROS generation

ROS generated upon direct exposure to rGO and rGO-P was assessed at two time points: 4h and 24h. It is seen from Figure 6a, PC-12 cells treated with rGO did not show an apparent increase in ROS production at 4h and 24h. However, rGO-P demonstrated a dose and time dependent increase in ROS generation. As the dose increased a gradual and statistically significant increase in ROS was noticed after 4h of exposure to rGO-P with respect to control. With prolonged exposure (24h) of rGO-P the fluorescence intensity increased in a dose dependent manner suggesting increased ROS generation (Figure 6b).

4.7 Acute toxicity in mice

rGO-P injected Swiss Albino mice did not show any signs of toxicity, morbidity or mortality after 72h of exposure *via* i.v. and i.p. route. Cage side observations for various factors such as change in skin and fur colour, eyes and mucous membrane, respiratory, circulatory and nervous

system and behaviour pattern did not show any visible alternations. This is shown in Table 1c.

The body weight changes in mice injected with 10mg/kg body weight of rGO-P administered through i.v. or i.p is shown in Figure 6c. No apparent change was observed in control and rGO-P injected animals at the end of 72h.

5. Discussion

Graphene is a promising material with myriad applications in the field of nanotechnology. The present study focuses on the green synthesis, characterization and neurotoxicity assessment of rGO-P. Currently, reduction of GO is the most widely used strategy for the fabrication of bulk amount of graphene called rGO. Although rGO is not defect free, it is highly processible and can be modified for various applications. Most of the chemical reducing agents used for the reduction of GO including hydrazine hydrate, sodium borohydride, hydrogen sulphide etc are highly dangerous and large scale production utilizing these agents are challenging. Ascorbic acid is a naturally occurring, eco-friendly alternative for reducing of GO to rGO [34]. Herein we employed ascorbic for the green synthesis of rGO. rGO is intrinsically insoluble in aqueous solution due to its hydrophobic nature. Pluronic P123 was utilized for non-covalent functionalization of rGO to aid in its stability in physiological solutions. The synthesis method is fairly simple, cost effective and superior yield was attained. It was noticed that 15mg of GO yielded ~13mg of rGO-P, which is much more than our previously established protocol.

Physico-chemical characterization of graphite, GO and rGO and rGO-P were performed to confirm the reduction efficiency, presence of impurities and attachment of Pluronic P123 in rGO-P. The oxidation and reduction process of graphite, GO and rGO was monitored by FTIR. The FTIR spectras indicates that GO was successfully reduced by ascorbic acid to rGO.

Stabilization of rGO-P with Pluronic P123 was assessed by comparing FTIR spectra of rGO, rGO-P and Pluronic P123.

Raman spectra are useful for characterizing graphitic material because it provides information on its structure and layer number. It was seen that highly ordered graphite shows a strong peak due to the in-plane vibration of graphite lattice ($\sim 1558\text{cm}^{-1}$) and a weak disorder band caused due to graphite edges ($\sim 1330\text{cm}^{-1}$) [31]. The occurrence of D band that becomes Raman active due to the presence of defects in rGO and rGO-P samples is indicative of defects in the graphitic plane as a result of the removal of oxygen. However, in this study, it is difficult to know the layer number as the samples were dried and the Raman spectra are resultant of several stacked sheets.

The peak area calculation of carbon and oxygen elements from the XPS spectra survey scan revealed that the C/O ratio increased from 1.88 in GO to 7.30 in rGO. This indicates that most of the oxygen moieties were removed in rGO upon reduction with ascorbic acid [35]. The introduction of Pluronic P123 caused the C/O ratio to decrease considerably. A significant difference can be observed between the C1s spectra of GO and rGO. GO and rGO contains sp^2 and sp^3 hybridized hydrocarbon peaks at $\sim 284.5\text{eV}$ and $\sim 285.0\text{eV}$ respectively [36]. However, GO shows an additional intense peak around $\sim 286.5\text{eV}$ due to the presence of hydroxyl or epoxy group (C-O) and less intense peaks around $\sim 288.9\text{eV}$ (carboxyl O=C-OH) and $\sim 287.0\text{eV}$ (carbonyl group C=O) indicating a considerable degree of oxidation. On the other hand, C1s spectra of rGO show less intense peak attributing to hydroxyl or epoxy group ($\sim 286.5\text{eV}$) and carboxyl group ($\sim 288.9\text{eV}$). This indicates that most of the oxygen moieties were removed upon reduction with a few residual oxygen functional groups.

TGA was carried out to analyze the reduction efficiency of GO to rGO and rGO-P. Graphite was highly stable up to 600°C beyond which temperature the bulk pyrolysis of the carbon

exoskeleton was observed [30]. The efficient reduction of GO using ascorbic acid was confirmed by analyzing the TGA curve of rGO. An enhanced thermal stability was observed for rGO and rGO-P suggesting complete removal of oxygen functional groups. Weight loss of rGO and rGO-P was observed from $>400^{\circ}\text{C}$ and is attributed to the pyrolysis of carbon [30]. This suggests that GO was reduced successfully to rGO and rGO-P.

XRD analysis further confirmed the reduction process by monitoring the crystalline structure of graphite, GO, rGO and rGO-P. The increase in interlayer spacing of GO (0.777nm) when compared to graphite (0.350nm) indicates the presence of oxygen moieties between the carbon lattice. Interlayer spacing of rGO decreased (0.336nm) during reduction process and suggested efficient deoxygenation of GO [24]. In rGO-P the interlayer spacing of 0.401nm was attributed to the intercalation of Pluronic P123 into the matrix [37].

TEM analysis was performed to further characterize the structure of rGO-P. The characteristic scrolled and wrinkled appearance to attain thermodynamic stability was noticed in rGO-P. Similar findings were reported by Wojtoniszak *et al* [30]. In addition to that, rGO-P shows round micellar structures of Pluronic P123 [38]. The hydrodynamic radius of rGO-P in water was assessed using DLS and the results are shown in Table 4.2 **Error! Reference source not found.** rGO-P showed a hydrodynamic radius of $784.03 \pm 17.10\text{nm}$ and poly dispersity index (PDI) of 0.43 ± 0.10 (table 1 d).

For *in vitro* biological studies, rGO and rGO-P were used. rGO served as an uncoated control to understand the possible differential response in the cells. The endotoxin content was estimated, since its presence can invalidate and produce erroneous results in biological studies. It was found that the endotoxin levels were ≤ 0.05 EU/ml for both. As per the USP guidelines (chapter 85, 2011) the recommended endotoxin levels for drugs and medical devices is 0.5 EU/ml for all routes of administration (except intrathecal). For intrathecal administrations it is

0.2 EU/ml. Therefore, it is safe to presume that rGO and rGO-P were endotoxin free and safe for biological applications.

Knowledge of the corona components will aid in understanding the fate of the nanoparticle within the biological system [33]. The protein concentration in the supernatant was decreased with increase in rGO and rGO-P concentration suggesting that both the nanomaterials promoted protein binding. Enhanced protein adsorption by rGO was noticed when compared to rGO-P. SDS-PAGE analysis showed protein corona formation in rGO with a noticeable band between 55 and 70kDa. Since the major protein present in serum is albumin. This protein was likely albumin (molecular weight of 66.5 kDa) that is most abundant in serum. Gu *et al* [39] demonstrated that protein corona formation in rGO was due to the π - π stacking interaction between aromatic residues in the protein and the sp^2 graphitic carbon. Protein corona formation was not detectable in rGO-P samples suggesting low protein adsorption. Reports suggest that nanomaterials functionalized with PEG evade the reticulo-endothelial system (RES) by preventing adsorption of proteins such as opsonins [40]. This implies that stabilizing with Pluronic P123 (containing two PEG moieties) prevented protein adsorption in rGO-P.

BBB acts as protective barrier for the nervous system against various invaders. NPs ability to cross BBB opens up scope for using NPs for drug delivery, imaging and regeneration at neuronal site. Graphene has been now widely been focused as a reliable material for various applications of neuroscience [41]. Previous literature suggests that graphene acts as an exceptional platform for adhesion, promote proliferation and differentiation of stem cells to neurons [42]. The increasing attractiveness of graphene for various healthcare applications imposes need to evaluate the compatibility of the material, possible interaction within the living

system or detect any neurophysiological changes induced by the NPs. The ability to cross BBB raises potential risk factors apart from the application merits. There are several reports on the neurotoxic effects of graphene. Bramini, M *et al.*, in 2016 reported the effect of exposure of few layer thick pristine graphene (PR) and single layer graphene oxide (GO) on rat primary cortical neurons. The results of the study revealed that though the graphene NPs internalized through the endolysosomal pathway did not induce any decrease in neuron viability, it caused inhibition of excitatory transmission as well as excitatory synaptic contacts reduction. GO NPs induced autophagy and disturbance in Ca²⁺ hemostasis [43]. The unwanted effect of graphene on neuronal interface demands a more comprehensive evaluation of the NPs. One of the ways to trackle the toxic effect of nanoparticles is by proper functionalization. Plurionics coating is a dependable functionalization for rGO before applying for various applications. Present study was designed to assess the compatibility of plurionics stabilized nanoparticles with neurons and whether the material induced any neurophysiological response in rejection to the material. *In vitro* toxicity studies provide a valuable tool to elucidate the mechanism of toxicity within a controlled environment. PC-12 cell viability and membrane damage after exposure to extract or upon direct contact of rGO and rGO-P were assessed using MTS assay and LDH release assay. Synthesis of rGO and rGO-P utilizes numerous chemicals. Presence of trace amount of the chemicals may cause toxicity to cells. To ensure safety, extracts of rGO and rGO-P were assessed for toxicity. rGO and rGO-P extracts (8h and 24h) did not cause any loss in cell viability or membrane damage after 24h exposure suggesting the absence of toxic chemicals. Toxicity of AgNP extracts (positive control) was due to leaching of silver ions in aqueous media. The concentration (5, 10, 20, 40 and 80µg/ml) chosen for direct contact assay were based on our previous work [44]. PC-12 cells after incubation with rGO and rGO-P for 24h showed a dose dependent toxicity. A similar dose-dependent response was reported in human ovarian cancer cell lines treated with uric acid rGO (UA-rGO) [45]. Mechanical disruption of

cell membrane due to direct contact with the nanomaterials results in leakage of LDH from the cell into the culture media. Since GFNs have sharp edges there is a possibility of cutting and disrupting the membrane and subsequently leading to LDH leakage [46]. rGO induced a dose dependent increase in LDH concentration in the media suggesting mechanical damage to the cells. The toxicity of rGO was consistent with results obtained while treating breast cancer cell lines with bacterially reduced GO [47]. However, rGO-P did not induce LDH release suggesting that the Pluronic P123 mitigated the membrane damaging effect.

Exposure to toxic materials results in changes in morphology of the cells. Cytoskeletal disruption in PC-12 cells was noticed at high concentrations of rGO exposure whereas rGO-P did not induce any visible change. This indicates that rGO might disrupt the neuronal processes as the concentration increases. Similar findings are shown by Li *et al.*, [48], where it was seen that plate-like graphene sheets physically disrupt the cytoskeletal organization in lung epithelial cells and macrophages. Chiacchiaretta *et al.*, reported that astrocytes when exposed to GO suffered actin fibre breakdown and relocation of α -tubulin. G-flakes internalization eventually lead to morphological changes due to cytoskeleton disruption [49]. The observation was correlated with results obtained from LDH release assay suggesting rGO induced membrane damage subsequently causing cytoskeletal disruption. The stabilization with Pluronic P123 may have ameliorated this effect in PC-12 cells.

One of the major developed paradigm from a mechanistic perspective of nanomaterial toxicity is ROS mediated oxidative stress [50]. The capacity of rGO and rGO-P to induce ROS after 4h and 24h exposure to PC-12 cells were analyzed. It was noticed that rGO did not promote ROS generation at 4h and 24h. A similar trend was observed in our previous study carried out in A549 cells [51]. Owing to the hydrophobic nature of rGO it is difficult to keep it dispersed in

the medium. This may cause aggregation and less interaction with cell and reduce the amount of ROS. Another possibility is ROS scavenging property of rGO as mentioned by Qiu *et al.*, [52]. It was suggested that graphene based materials show superior ROS scavenging properties associated with its sp² carbon network. Further studies are required to confirm these findings. Contrary to rGO, rGO-P was capable of inducing dose and time dependent increase in ROS in PC-12 cells suggesting oxidative stress mediated toxicity of rGO-P. The presence of Pluronic P123 in rGO-P maintains colloidal stability and may have hindered the ROS scavenging property by concealing the graphitic networks.

Since *in vitro* studies indicated the potential toxic effect of rGO-P to neuronal cells, *in vivo* studies were performed to understand the acute toxic effect after i.v. and i.p. administration of rGO-P. Animals were administered 10mg/kg body weight based on literature survey and clinically relevant dose [53]. An acute toxicity study was designed to evaluate the systemic response in Swiss Albino mice after i.v. and i.p. injection of rGO-P for a period of 72h. The cage side observation of rGO-P exposed mice showed no alterations in clinical symptoms such as change in skin colour, fur coat, eye and mucous membrane, respiration, gastrointestinal tract and so on. Moreover, behaviour patterns were similar to that on control animals. This suggests that there were no complications associated with the administration of rGO-P. Behavior is a gross measure of the integration of neural function. Similar results were observed by Mendonca *et al* [54] after injection of rGO in rats. Current *in vivo* data are not enough to give real information about the neurotoxicity of the rGO-P. More comprehensive studies recommended for getting a clearer picture on neurotoxicity. From the current results, mice exposed to rGO-P *via* i.v. and i.p. did not show any weight loss indicating the animals were healthy and did not show any rGO-P related adverse effects.

6. Conclusion

The study shows a facile and inexpensive method for the bulk synthesis of well dispersed rGO-P. Moreover, incorporating a naturally occurring antioxidant ascorbic acid as reducing agent makes the synthesis process environmentally friendly facilitating large scale production. Utilizing Pluronic P123 as the stabilizing agent aided in superior yield (~ 80% yield) of highly dispersed rGO-P that is useful for biological applications. The results of the *in vitro* toxicity assays indicated that rGO-P shows dose dependent cytotoxicity and oxidative stress after 24h exposure to differentiated PC-12 cells. However, administration of rGO-P by i.v. and i.p. injection to Swiss albino mice did not show any pronounced toxicity after 72h. In conclusion, rGO-P was successfully synthesized and characterized and showed a slight dose dependent cytotoxicity in *in vitro* conditions. Nonetheless, it showed no prominent toxicity *in vivo*. Further studies should be carried out to elucidate the long-term effect of rGO-P on the biological system.

7. Conflict of interest

The authors declare that there is no conflict of interest.

8. Acknowledgement

The authors express their sincere thanks to The Director and Head, Biomedical Technology Wing, Sree Chitra Tirunal Institute for Medical Sciences and Technology, Thiruvananthapuram for their support and for providing the infrastructure to carry out this work. The authors are thankful to Commonwealth Scholarship Committee, United Kingdom for the providing the grant to carry out part of the work. RSC thanks Indian Council of Medical Research (ICMR), New Delhi for the Senior Research Fellowship.

Reference

[1] Allen, M.J., Tung, V.C. and Kaner, R.B., 2009. Honeycomb carbon: a review of graphene. *Chemical reviews*, 110(1), 132-145.

- [2] Choi, W., Lahiri, I., Seelaboyina, R. and Kang, Y.S., 2010. Synthesis of graphene and its applications: a review. *Critical Reviews in Solid State and Materials Sciences*, 35(1), 52-71.
- [3] Chang, H. and Wu, H., 2013. Graphene-based nanomaterials: synthesis, properties, and optical and optoelectronic applications. *Advanced Functional Materials*, 23(16), 1984-1997.
- [4] Rahman, M., Akhter, S., Ahmad, M.Z., Ahmad, J., Addo, R.T., Ahmad, F.J. and Pichon, C., 2015. Emerging advances in cancer nanotheranostics with graphene nanocomposites: opportunities and challenges. *Nanomedicine*, 10(15), 2405-2422.
- [5] Rahman, M., Zaki Ahmad, M., Ahmad, J., Firdous, J., Jalees Ahmad, F., Mushtaq, G., A Kamal, M. and Akhter, S., 2015. Role of graphene nano-composites in cancer therapy: theranostic applications, metabolic fate and toxicity issues. *Current drug metabolism*, 16(5), 397-409.
- [6] Rahman, M., Ahmad, M.Z., Kazmi, I., Akhter, S., Afzal, M., Gupta, G., Jalees Ahmed, F. and Anwar, F., 2012. Advancement in multifunctional nanoparticles for the effective treatment of cancer. *Expert opinion on drug delivery*, 9(4), 367-381.
- [7] Chang, H. and Wu, H., 2013. Graphene-based nanomaterials: synthesis, properties, and optical and optoelectronic applications. *Advanced Functional Materials*, 23(16), 1984-1997.
- [8] Pei, S. and Cheng, H.M., 2012. The reduction of graphene oxide. *Carbon*, 50(9), pp.3210-3228.
- [9] Zhang, J., Yang, H., Shen, G., Cheng, P., Zhang, J. and Guo, S., 2010. Reduction of graphene oxide via L-ascorbic acid. *Chemical Communications*, 46(7), 1112-1114.
- [10] De Silva, K.K.H., Huang, H.H. and Yoshimura, M., 2018. Progress of reduction of graphene oxide by ascorbic acid. *Applied Surface Science*, 447, 338-346.
- [11] Y-K. Kim, M-H. Kim, D-H. Min. Biocompatible reduced graphene oxide prepared by using dextran as a multifunctional reducing agent. *Chem. Commun.* **2011**, 47, 3195-3197.

- [12] S-Z. Zu, B-H. Han. Aqueous dispersion of graphene sheets stabilized by pluronic copolymers: formation of supramolecular hydrogel. *J. Phys. Chem. C.* **2009**, 113, 13651-13657.
- [13] J. T. Robinson, S. M. Tabakman, Y. Liang, H. Wang, H.C. Sanchez, D. Vinh, H. Dai. Ultrasmall reduced graphene oxide with high near-infrared absorbance for photothermal therapy. *J. Am. Chem. Soc.* **2011**, 133, 6825-6831.
- [14] A. K. Swain, D. Bahadur. Enhanced stability of reduced graphene oxide colloid using cross-linking polymers. *J. Phys. Chem. C.* **2014**, 118, 9450-9457.
- [15] Georgakilas, V., Otyepka, M., Bourlinos, A.B., Chandra, V., Kim, N., Kemp, K.C., Hobza, P., Zboril, R. and Kim, K.S., 2012. Functionalization of graphene: covalent and non-covalent approaches, derivatives and applications. *Chemical reviews*, 112(11), 6156-6214.
- [16] Zu, S.Z. and Han, B.H., 2009. Aqueous dispersion of graphene sheets stabilized by pluronic copolymers: formation of supramolecular hydrogel. *The Journal of Physical Chemistry C*, 113(31), 13651-13657.
- [17] Fadeel, B., Bussy, C., Merino, S., Vázquez, E., Flahaut, E., Mouchet, F., Evariste, L., Gauthier, L., Koivisto, A.J., Vogel, U. and Martin, C., 2018. Safety Assessment of Graphene-Based Materials: Focus on Human Health and the Environment. *ACS nano*, 12(11),10582-10620.
- [18] Bramini, M., Alberini, G., Colombo, E., Chiacchiarretta, M., DiFrancesco, M.L., Maya-Vetencourt, J.F., Maragliano, L., Benfenati, F. and Cesca, F., 2018. Interfacing Graphene-Based Materials With Neural Cells. *Frontiers in systems neuroscience*, 12, 12.
- [19] Rahman M, Beg S, Ahmad MZ, Anwar F and Kumar V. Graphenes & Their Applications in Healthcare Systems. Graphene Science Handbook Size-Dependent Properties, 397-414 CRC Press 2016.
- [20] a) Rauti, R., Lozano, N., León, V., Scaini, D., Musto, M., Rago, I., Ulloa Severino, F.P., Fabbro, A., Casalis, L., Vázquez, E. and Kostarelos, K., 2016. Graphene oxide nanosheets

reshape synaptic function in cultured brain networks. *ACS nano*, *10*(4), 4459-4471. b) Bramini, M., Sacchetti, S., Armirotti, A., Rocchi, A., Vázquez, E., León Castellanos, V., Bandiera, T., Cesca, F. and Benfenati, F., 2016. Graphene oxide nanosheets disrupt lipid composition, Ca²⁺ homeostasis, and synaptic transmission in primary cortical neurons. *ACS nano*, *10*(7), 7154-7171. c) Chiacchiaretta, M., Bramini, M., Rocchi, A., Armirotti, A., Giordano, E., Vázquez, E., Bandiera, T., Ferroni, S., Cesca, F. and Benfenati, F., 2018. Graphene oxide upregulates the homeostatic functions of primary astrocytes and modulates astrocyte-to-neuron communication. *Nano letters*, *18*(9), 5827-5838.

[21] Mendonça, M.C.P., Soares, E.S., de Jesus, M.B., Ceragioli, H.J., Ferreira, M.S., Catharino, R.R. and Cruz-Höfling, M.A., 2015. Reduced graphene oxide induces transient blood–brain barrier opening: an in vivo study. *Journal of nanobiotechnology*, *13*(1), 78.

[22] W. S. Hummers, R. E. Offeman. Preparation of graphitic oxide. *J. Am. Chem. Soc.* **1958**, *80*, 1339-1339.

[23] S-Z. Zu, B-H. Han. Aqueous dispersion of graphene sheets stabilized by pluronic copolymers: formation of supramolecular hydrogel. *J. Phys. Chem. C.* **2009**, *113*, 13651-13657.

[24] A. Jedlovszky-Hajdu, F. B. Bombelli, M. P. Monopoli, E. Tombacz, K. A. Dawson. Surface coatings shape the protein corona of SPIONs with relevance to their application in vivo. *Langmuir* **2012**, *28*, 14983-91.

[25] O. H. Lowry, N. J. Rosebrough, A. L. Farr, R. J. Randall. Protein measurement with the folin phenol reagent. *J. Biol. Chem.* **1951**, *193*, 265-75.

[26] Zhang, T., Wang, L., Chen, Q. and Chen, C., 2014. Cytotoxic potential of silver nanoparticles. *Yonsei medical journal*, *55*(2), 283-291.

- [27] E-Y. Choi, T. H. Han, J. Hong, J. E. Kim, S. H. Lee, H. W. Kim, S. O. Kim. Noncovalent functionalization of graphene with end-functional polymers. *J. Mater. Chem.* 2010, 20, 1907-1912.
- [28] C. Xu, X. Shi, A. Ji, L. Shi, C. Zhou, Y. Cui. Fabrication and characteristics of reduced graphene oxide produced with different green reductants. *PLoS. One.* **2015**, 10, e0144842.
- [29] M. Pudukudy, Z. Yaakob. Hydrothermal synthesis of mesostructured ZnO micropylramids with enhanced photocatalytic performance. *Superlattices. Microst.* **2013**, 63, 47-57.
- [30] M. Wojtoniszak, X. Chen, R. J. Kalenczuk, A. Wajda, J. Łapczuk, M. Kurzewski, M. Drozdziak, P. K. Chu, E. Borowiak-Palen. Synthesis, dispersion, and cytocompatibility of graphene oxide and reduced graphene oxide. *Colloids. Surf. B. Biointerfaces.* **2012**, 89, 79-85.
- [31] K. N. Kudin, B. Ozbas, H. C. Schniepp, R. K. Prud'homme, I. A. Aksay, R. Car. Raman spectra of graphite oxide and functionalized graphene sheets. *Nano. Lett.* **2008**, 8, 36-41.
- [32] E-Y. Choi, T. H. Han, J. Hong, J. E. Kim, S. H. Lee, H. W. Kim, S. O. Kim. Noncovalent functionalization of graphene with end-functional polymers. *J. Mater. Chem.* **2010**, 20, 1907-1912.
- [33] Castagnola, V., Zhao, W., Boselli, L., Giudice, M.L., Meder, F., Polo, E., Paton, K.R., Backes, C., Coleman, J.N. and Dawson, K.A., 2018. Biological recognition of graphene nanoflakes. *Nature communications*, 9(1), 1577.
- [34] J. Zhang, H. Yang, G. Shen, P. Cheng, J. Zhang, S. Guo. Reduction of graphene oxide via L-ascorbic acid. *Chem. Commun.* **2010**, 46, 1112-1114.
- [35] G. Sobon, J. Sotor, J. Jagiello, R. Kozinski, M. Zdrojek, M. Holdynski, P. Paletko, J. Boguslawski, L. Lipinska, K. M. Abramski, Graphene oxide versus reduced graphene oxide as saturable absorbers for Er-doped passively mode-locked fiber laser. *Opt. Express.* **2012**, 20, 19463-73.

- [36] S. Drewniak, R. Muzyka, A. Stolarczyk, T. Pustelny, M. Kotyczka-Moranska, M. Setkiewicz. Studies of reduced graphene oxide and graphite oxide in the aspect of their possible application in gas sensors. *Sensors. (Basel)*. **2016**, 16.
- [37] B. Gupta, N. Kumar, K. Panda, A. A. Melvin, S. Joshi, S. Dash, A. K. Tyagi. Effective noncovalent functionalization of poly (ethylene glycol) to reduced graphene oxide nanosheets through γ -radiolysis for enhanced lubrication. *J. Phys. Chem. C*. **2016**, 120, 2139-2148.
- [38] N. Kundu, A. Roy, D. Banik, J. Kuchlyan, N. Sarkar. Graphene Oxide and pluronic copolymer aggregates—possible route to modulate the adsorption of fluorophores and imaging of live cells. *J. Phys. Chem. C*. **2015**, 119, 25023-25035.
- [39] Z. Gu, Z. Yang, L. Wang, H. Zhou, C. A. Jimenez-Cruz, R. Zhou. The role of basic residues in the adsorption of blood proteins onto the graphene surface. *Sci. Rep.* **2015**, 5, 10873.
- [40] B. Pelaz, P. Del Pino, P. Maffre, R. Hartmann, M. Gallego, S. Rivera-Fernández, J. M. De La Fuente, G. U. Nienhaus, W. J. Parak. Surface functionalization of nanoparticles with polyethylene glycol: effects on protein adsorption and cellular uptake. *ACS. Nano*. **2015**, 9, 6996-7008.
- [41] Zhang, Y., Nayak, T.R., Hong, H. and Cai, W., 2012. Graphene: a versatile nanoplatform for biomedical applications. *Nanoscale*, 4(13), 3833-3842.
- [42] Gardin, C., Piattelli, A. and Zavan, B., 2016. Graphene in regenerative medicine: focus on stem cells and neuronal differentiation. *Trends in biotechnology*, 34(6), 435-437.
- [43] Bramini, M., Sacchetti, S., Armirotti, A., Rocchi, A., Vázquez, E., León Castellanos, V., Bandiera, T., Cesca, F. and Benfenati, F., 2016. Graphene oxide nanosheets disrupt lipid composition, Ca²⁺ homeostasis, and synaptic transmission in primary cortical neurons. *ACS nano*, 10(7), 7154-7171.

- [44] S. C. Reshma, S. Syama, P. V. Mohanan, Nano-biointeractions of PEGylated and bare reduced graphene oxide on lung alveolar epithelial cells: A comparative in vitro study. *Colloids. Surf. B. Biointerfaces*. **2016**, 140, 104-16.
- [45] Y. J. Choi, E. Kim, J. Han, J. H. Kim, S. Gurunathan, A novel biomolecule-mediated reduction of graphene oxide: a multifunctional anti-cancer agent. *Molecules*. **2016**, 21, 375.
- [46] O. Akhavan, E. Ghaderi, Toxicity of graphene and graphene oxide nanowalls against bacteria. *ACS. Nano*. **2010**, 4, 5731-5736.
- [47] S. Gurunathan, J. W. Han, V. Eppakayala, J. H. Kim. Green synthesis of graphene and its cytotoxic effects in human breast cancer cells. *Int. J. Nanomedicine*. **2013**, 8, 1015-1027.
- [48] Y. Li, Y. Liu, Y. Fu, T. Wei, L. Le Guyader, G. Gao, R. S. Liu, Y. Z. Chang, C. Chen, The triggering of apoptosis in macrophages by pristine graphene through the MAPK and TGF-beta signaling pathways. *Biomaterials*. **2012**, 33, 402-11.
- [49] Chiacchiaretta, M., Bramini, M., Rocchi, A., Armirotti, A., Giordano, E., Vázquez, E., Bandiera, T., Ferroni, S., Cesca, F. and Benfenati, F., 2018. Graphene oxide upregulates the homeostatic functions of primary astrocytes and modulates astrocyte-to-neuron communication. *Nano letters*, 18(9), 5827-5838.
- [50] A. Nel, T. Xia, L. Madler, N. Li. Toxic potential of materials at the nanolevel. *Science*, **2006**, 311, 622-7.
- [51] Y. Qiu, Z. Wang, A. C. E. Owens, I. Kulaots, Y. Chen, A. B. Kane, R. H. Hurt. Antioxidant chemistry of graphene-based materials and its role in oxidation protection technology. *Nanoscale*, **2014**, 6, 11744-11755.
- [52] S. Kanakia, J. D. Toussaint, S.M. Chowdhury, T. Tembulkar, S. Lee, Y. P. Jiang. Dose ranging, expanded acute toxicity and safety pharmacology studies for intravenously administered functionalized graphene nanoparticle formulations. *Biomaterials*, **2014**, 35

[53] M. C. Mendonça, E. S. Soares, M. B. de Jesus, H. J. Ceragioli, S. P. Irazusta, Â. G. Batista, M. A. Vinolo, M. R. Maróstica Júnior, M. A. Da Cruz-Höfling. Reduced graphene oxide: nanotoxicological profile in rats. *J. Nanobiotechnology*. **2016**,14, 53

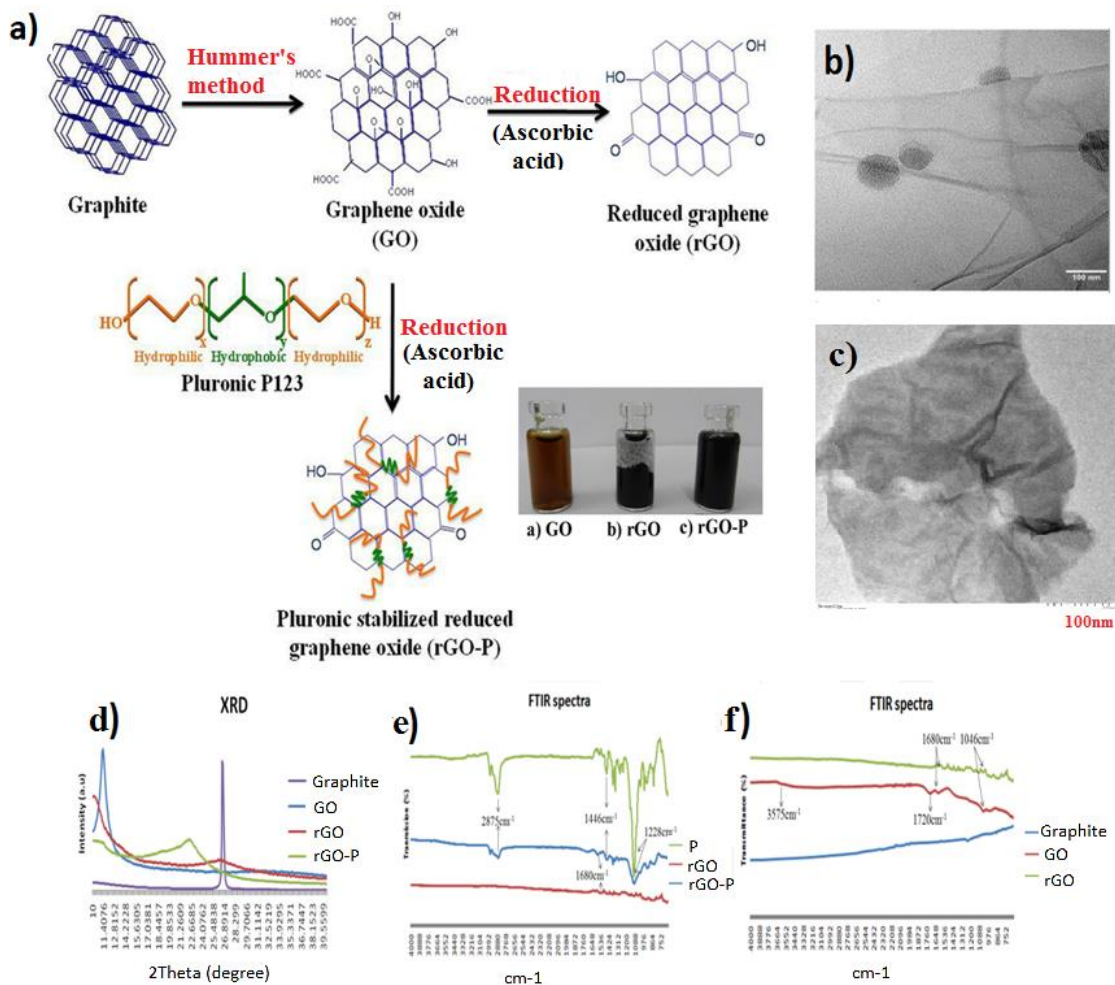


Figure 1: Synthesis of rGO and rGO-P from GO. Inset shows a)GO; b)rGO and c)rGO-P solutions. b)TEM image of rGO-P. c) TEM image of rGO. d) XRD spectra of graphite, GO, rGO, rGO-P. e) FT-IR spectra of Pluronic (P), rGO, rGO-P. f) FT-IR spectra of graphite, GO, rGO.

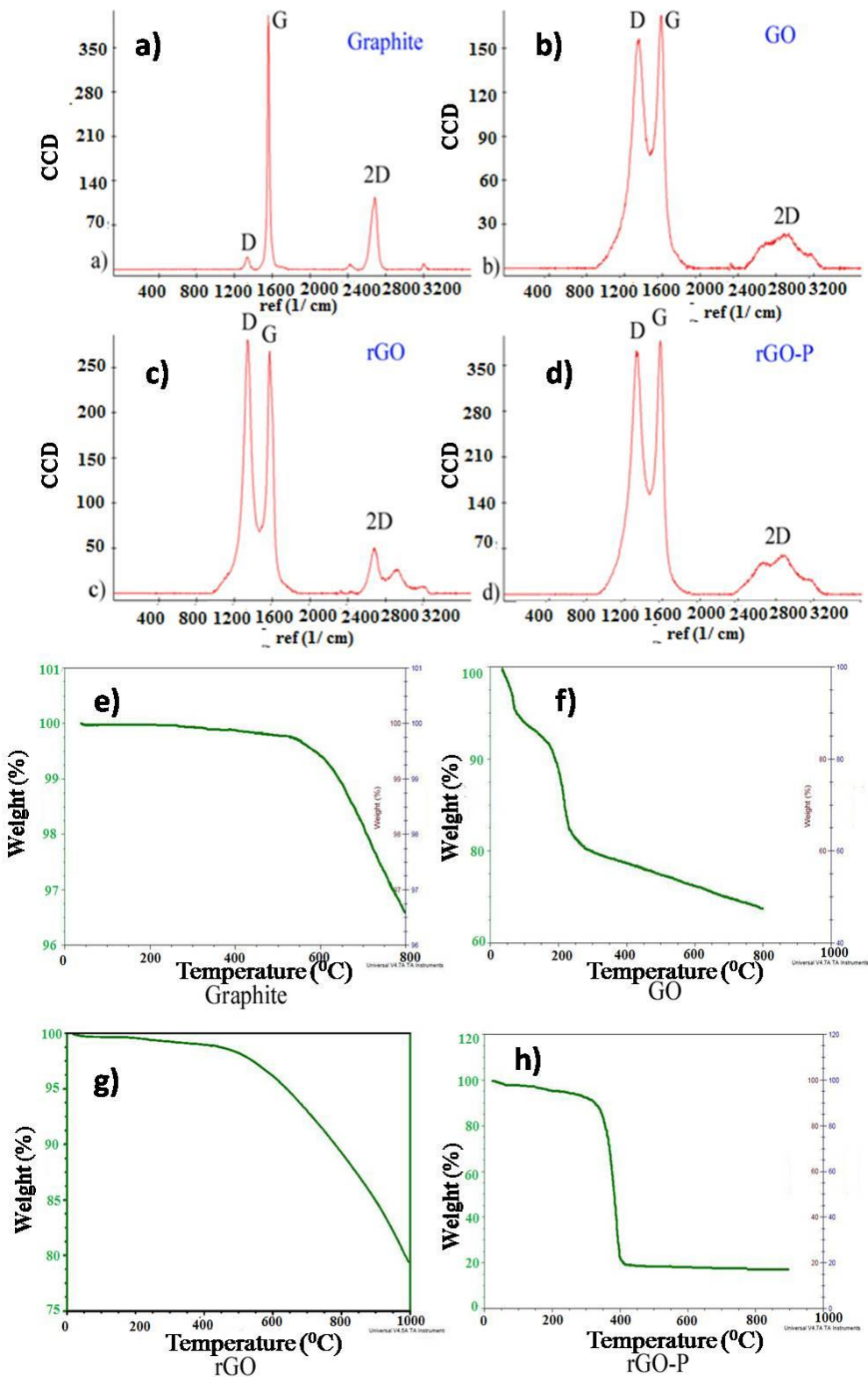
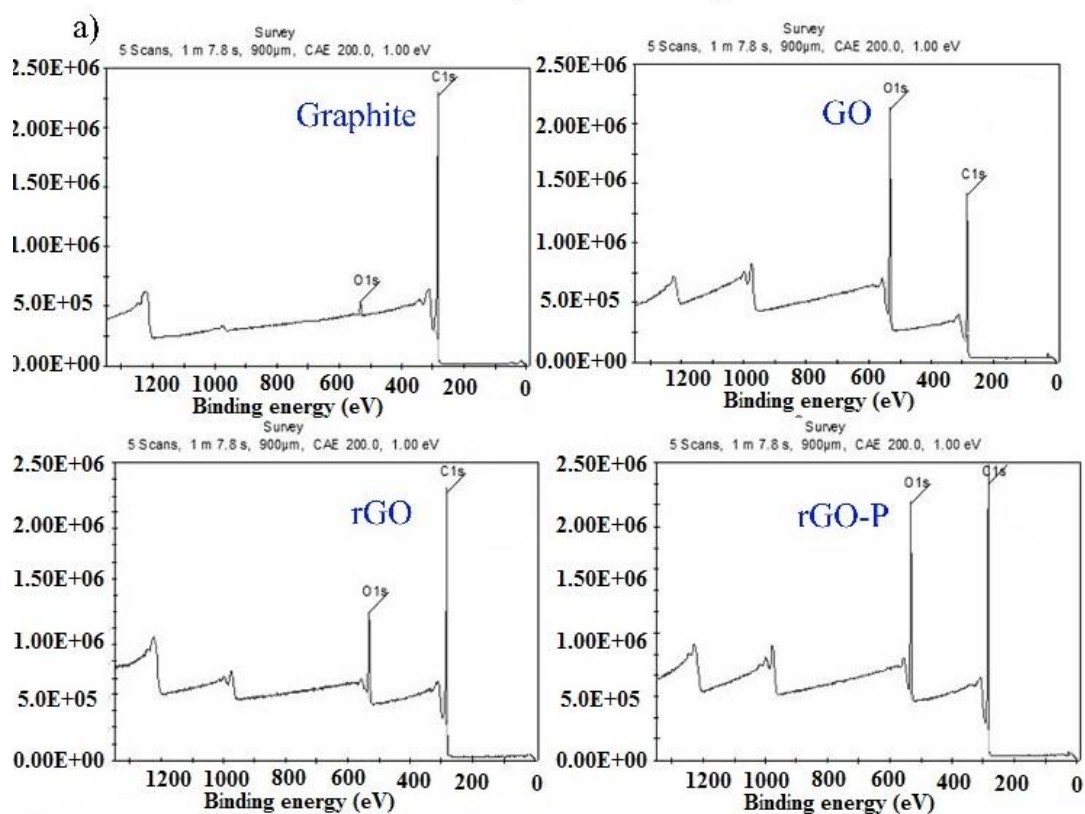


Figure 2: a-d) Raman spectrum of graphite, GO, rGO and rGO-P. e-h) TGA analysis of Graphite, GO, rGO and rGO-P;

XPS survey scan analysis



b) XPS C1s core spectra

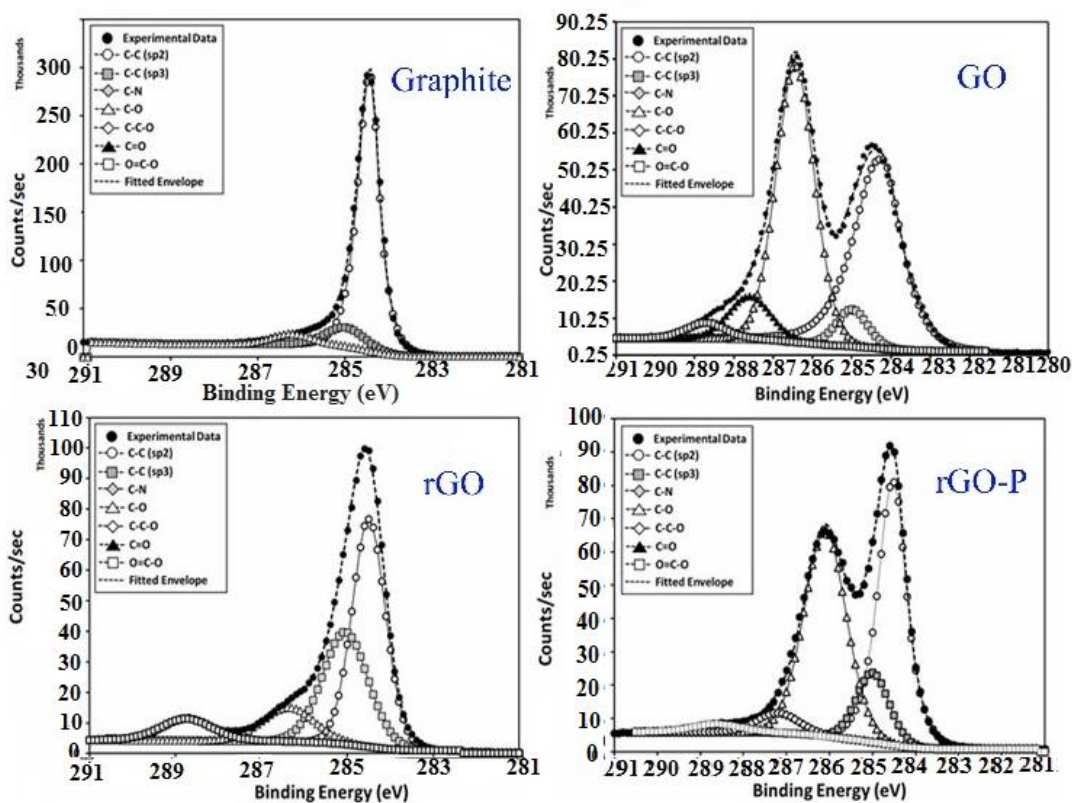


Figure 3: a) XPS survey scan spectra of Graphite, GO, rGO and rGO-P and b) XPS C1s core spectra of Graphite, GO, rGO and rGO-P

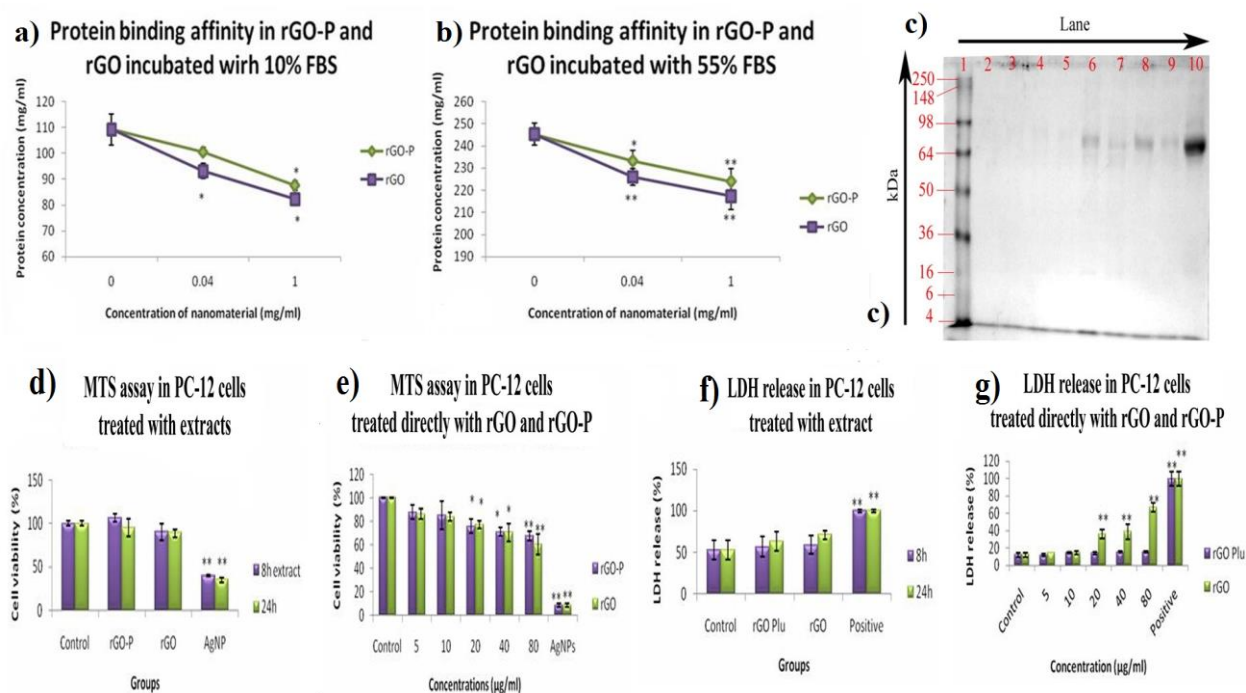


Figure 4: Protein corona formation in rGO and rGO-P. Protein concentration in supernatant of rGO and rGO-P incubated with a) 10% FBS, b) 55% FBS and c) gel electrophoresis of protein corona. Lane 1-marker, Lane 2- 1mg/ml rGO-P in 10% FBS; Lane 3- 0.04mg/ml rGO-P in 10% FBS; lane 4- 1mg/ml rGO-P in 55% FBS; lane 5- 0.04mg/ml rGO-P in 55% FBS ; lane 6-/ml rGO in 10% FBS;lane 7-0.04mg/ml rGO in 10% FBS ; lane 8 -1mg/ml rGO in 55% FBS ;lane9- 0.04mg/ml rGO in 55% FBS ;lane 10- 0.04mg/ml rGO in 55% FBS. * represent p value <0.05 and ** represents p value < 0.001. d) MTS assay of 8h and 24h extract of rGO and rGO-P in PC-12 cells. Untreated cells were kept as control and AgNP extract treated cells as positive control. ** denotes p <0.001; e) Direct contact MTS assay of rGO and rGO-P for 24 h in PC-12 cells. Untreated cells were kept as control and AgNP treated cells as positive control.* denotes p < 0.05 and **<0.001; f) LDH assay of 8h and 24h extract of rGO and rGO-P in PC-12 cells. Untreated cells were kept as control and lysed cells as positive control. ** denotes p <0.001 and g) Direct contact LDH assay of 8h and 24h of rGO and rGO-P in PC-12 cells. Untreated cells were kept as control and lysed cells as positive control. ** denotes p <0.001.

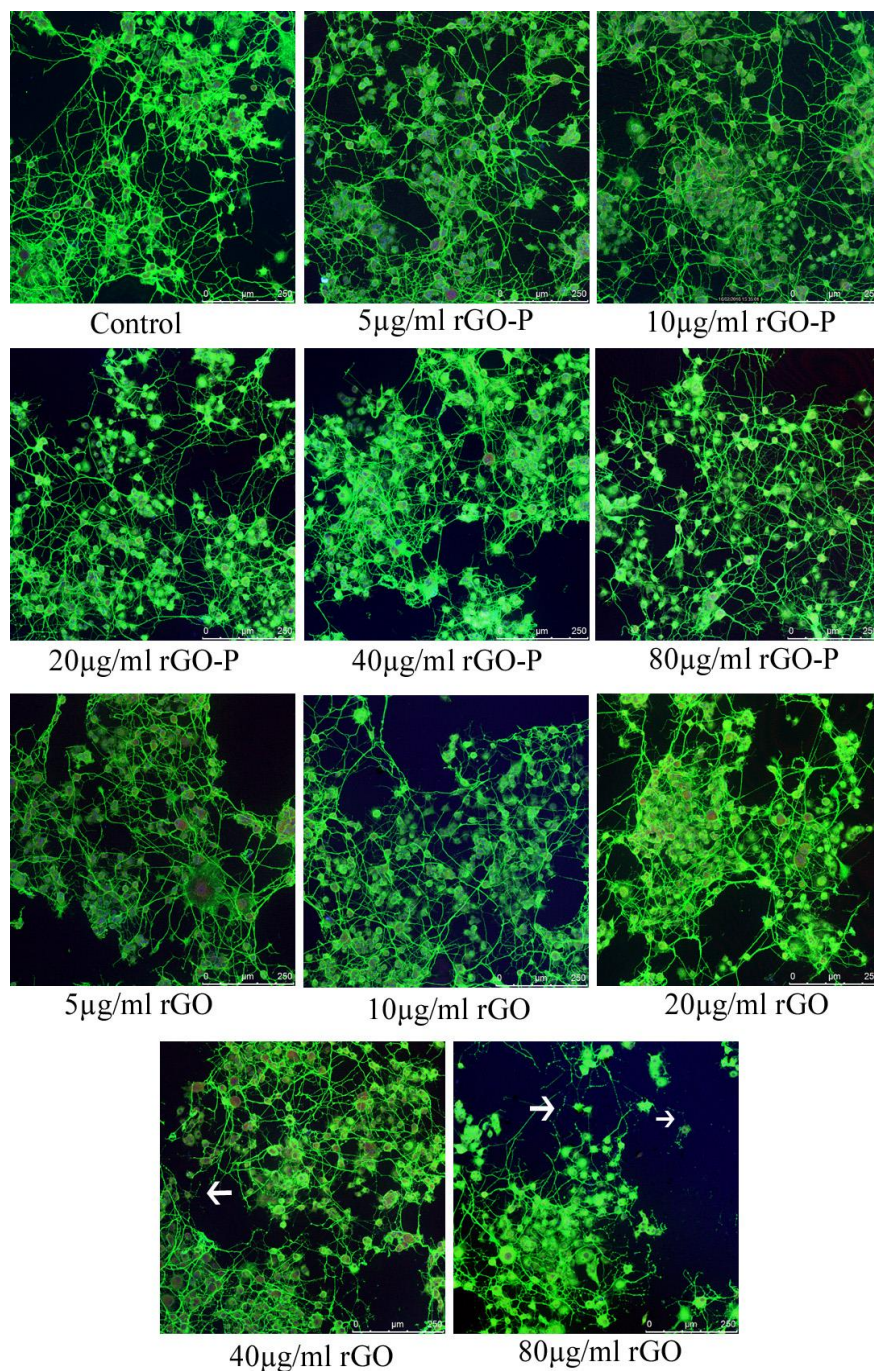


Figure 5: Morphology analysis of PC-12 cells treated for 24 h with rGO and rGO-P by staining with β -III tubulin. Cells with any treatment were taken as control. Arrows indicate cytoskeletal disruption. Scale: 250 μ m

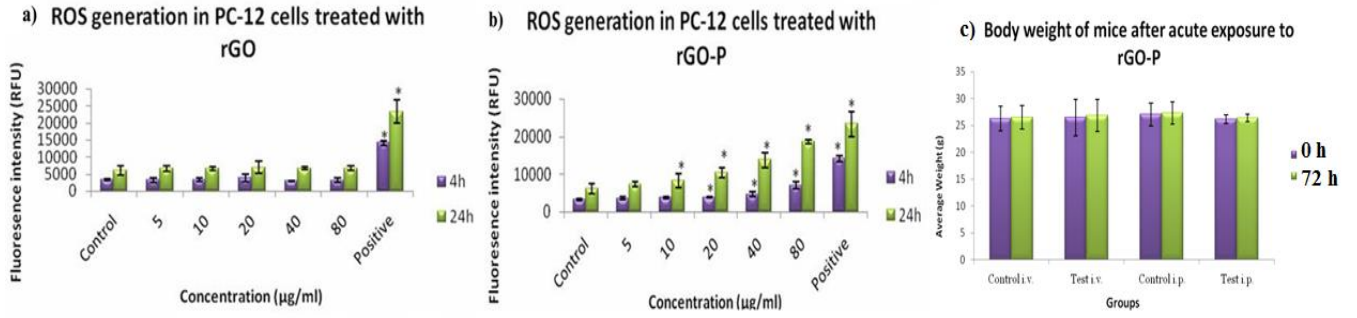


Figure 6: ROS generation in PC-12 cells treated with rGO and rGO-P for a) 4h and b) 24h. Untreated cells were kept as control and 100 μM H_2O_2 was kept as positive control. * denotes $p < 0.05$. c) Body weight of mice after acute exposure of rGO-P *via* i.v. and i.p. route at 0 h and after 72 h particle treatment.

a)

Sample	O1s	C1s	C/O
Graphite	2.1	97.9	46.17
GO	34.7	65.3	1.88
rGO	12	88	7.3
rGO-P	20.9	79.1	3.78

b)

Nanomaterials	Endotoxin content (EU/ml)
rGO-P	≤ 0.05
rGO	≤ 0.05

c)

Dose (10mg/kg body weight)		Clinical symptoms									
		1	2	3	4	5	6	7	8	9	10
Intravenous (i.v.) route	24h	N	N	N	N	N	N	N	N	N	N
	48h	N	N	N	N	N	N	N	N	N	N
	72h	N	N	N	N	N	N	N	N	N	N
Intraperitoneal (i.p.) route	24h	N	N	N	N	N	N	N	N	N	N
	48h	N	N	N	N	N	N	N	N	N	N
	72h	N	N	N	N	N	N	N	N	N	N

d)

Particle	Hydrodynamic radius (nm)	Poly dispersity index (PDI)
rGO-P	784.03\pm17.10	0.43\pm0.10

Table 1: a) The atomic percentage of oxygen and carbon and the C/O ratio of graphite, GO, rGO and rGO-P. b) Endotoxin content in rGO and rGO-P. c) Clinical symptoms in mice treated with treated with rGO-P for 72h. Response: 1. Respiratory; 2. Motor; 3. Convulsion; 4. Reflexes; 5. Ocular signs; 6. Cardiovascular signs; 7. Salivation; 8. Piloerection; 9. Analgesia and 10. Gastrointestinal. N=Normal. d) Poly dispersity index